Asymmetric nuclear matter based on chiral two- and three-nucleon interactions

C. Drischler,* K. Hebeler,† and A. Schwenk‡
Institut für Kernphysik, Technische Universität Darmstadt, 64289 Darmstadt, Germany
and ExtreMe Matter Institute EMMI, GSI Helmholtzzentrum für Schwerionenforschung GmbH, 64291 Darmstadt, Germany
(Received 26 October 2015; published 10 May 2016)

We calculate the properties of isospin-asymmetric nuclear matter based on chiral nucleon-nucleon (NN) and three-nucleon (3N) interactions. To this end, we develop an improved normal-ordering framework that allows us to include general 3N interactions starting from a plane-wave partial-wave-decomposed form. We present results for the energy per particle for general isospin asymmetries based on a set of different Hamiltonians, study their saturation properties, the incompressibility, symmetry energy, and also provide an analytic parametrization for the energy per particle as a function of density and isospin asymmetry.

DOI: 10.1103/PhysRevC.93.054314

I. INTRODUCTION

Microscopic calculations of isospin-asymmetric nuclear matter are important for nuclear physics and astrophysical applications. They allow to give *ab initio* constraints for key quantities for our understanding of core-collapse supernovae and neutron stars. In addition, they can guide energy-density functionals for global predictions of nuclear properties.

Advances in chiral effective field theory (EFT) [1,2] and renormalization group methods [3,4] have opened the way to improved and systematic studies of nuclear matter as well as finite nuclei [5,6]. For symmetric matter it was found that low-momentum nucleon-nucleon (NN) plus three-nucleon (3N) interactions are capable of predicting realistic saturation properties, with 3N forces fit only to few-body data [7], whereas neutron matter was found to be perturbative [8]. In subsequent studies, symmetric matter and neutron matter were also investigated based on chiral EFT interactions within the self-consistent Green's function framework [9,10], using coupled-cluster theory [11,12], with in-medium chiral perturbation theory [13] and in many-body perturbation theory [14]. Furthermore, the development of novel local chiral NN forces opened the way to first quantum Monte Carlo studies of neutron matter based on chiral EFT interactions [15–18]. The results of these studies also represent first nonperturbative validation of many-body perturbation theory for neutron matter.

Asymmetric nuclear matter has been studied within various many-body approaches during the last decades based on phenomenological NN potentials [19–25]. Chiral EFT interactions have been applied to asymmetric matter only recently [26–28]. Explicit calculations at general proton fractions allow us to extract key quantities like the nuclear symmetry energy more microscopically, because no empirical parametrizations for the energy as a function of the isospin asymmetry are needed. Commonly, such parametrizations were either based on the standard quadratic expansion (see, e.g., Ref. [27] for a recent work) or inspired by the form of energy-density functionals (see, e.g., Ref. [29]).

A major challenge for performing such many-body calculations is the treatment of 3N forces and the quantification of theoretical uncertainties. In contrast to many-body uncertainties, which can be investigated by benchmarking, the quantification of uncertainties in the nuclear Hamiltonian is a more challenging task (see, e.g., Ref. [30]). There are currently ongoing efforts to develop novel chiral EFT interactions (see, e.g., Refs. [31–33]) that enable order-by-order studies of matter and nuclei in the chiral expansion and allow us to test the validity of the chiral power counting at nuclear densities in a systematic way.

For these investigations 3N forces play a central role. In Weinberg power counting the leading 3N forces at next-to-next-to-leading order (N^2LO) contain two unknown low-energy couplings c_D and c_E, whereas the subleading 3N forces at next-to-next-to-next-to-leading order (N^3LO) do not contain any new low-energy couplings [34,35]. The first full N^3LO calculations of neutron matter showed that subleading 3N forces at N^3LO provide significant contributions to the energy per particle [36,37]. This could be an indication for a slow convergence of the chiral expansion for 3N forces. These findings were confirmed by first explorative calculations of symmetric matter up to N^3LO [37]. Due to the complexity and rich analytical structure of 3N forces at N^3LO [34,35,38] the 3N contributions at this order could only be included in the Hartree–Fock approximation in these studies. While this approximation is expected to be reasonable for neutron matter, such a treatment is certainly not reliable for sufficiently large proton fractions and consequently higher-order many-body contributions need to be included. For the same reason the calculations of asymmetric nuclear matter of Ref. [26] were limited to small proton fractions.

In this paper, we present a framework that allows us to include general 3N forces in calculations of asymmetric nuclear matter systematically and hence allows us to extend the studies of Ref. [26] to arbitrary proton fractions. Our calculations are based on a set of seven Hamiltonians with NN interactions at N^3LO evolved with the similarity renormalization group (SRG) to different resolution scales λ plus 3N interactions at N^2LO with 3N cutoff Λ_{3N}:

$$H(\lambda,\Lambda_{3N}) = T + V_{NN}(\lambda) + V_{3N}(\Lambda_{3N}). \quad (1)$$

*christian.drischler@physik.tu-darmstadt.de
†kai.hebeler@physik.tu-darmstadt.de
‡schwenk@physik.tu-darmstadt.de

TABLE I. The set of seven Hamiltonians used for the many-body calculations of this study. The low-energy couplings c_D, c_E were fit in Ref. [7] to the binding energy of ^{3}H and the charge radius of ^{4}He for given SRG resolution scale λ, 3N cutoff Λ_{3N}, and the long-range couplings c_i. The Hamiltonians are based on the N^{3}LO NN potential EM 500 MeV [39], except for Hamiltonian 6*, which is based on the N^{3}LO NN potential EGM 550/600 MeV [40]. Moreover, the Hamiltonians use consistent c_i values in NN and 3N interactions, except for Hamiltonian 7, which uses the c_i values from the NN partial-wave analysis of Ref. [41] in 3N interactions. We refer to Sec. IV B for a discussion of the special treatment of Hamiltonian 6*.

	NN potential	λ/Λ_{3N} [fm^{-1}]	c_1 [GeV^{-1}]	c_3 [GeV^{-1}]	c_4 [GeV^{-1}]	c_D	c_E
#1	EM 500 MeV	1.8/2.0	−0.81	−3.2	5.4	1.264	−0.120
#2	EM 500 MeV	2.0/2.0	−0.81	−3.2	5.4	1.271	−0.131
#3	EM 500 MeV	2.0/2.5	−0.81	−3.2	5.4	−0.292	−0.592
#4	EM 500 MeV	2.2/2.0	−0.81	−3.2	5.4	1.214	−0.137
#5	EM 500 MeV	2.8/2.0	−0.81	−3.2	5.4	1.278	−0.078
#6*	EGM 550/600 MeV	2.0/2.0	−0.81	−3.4	3.4	−4.828	−1.152
#7	EM 500 MeV	2.0/2.0	−0.76	−4.78	3.96	−3.007	−0.686

By using 3N forces at N^{2}LO as a truncated basis and assuming the long-range couplings c_i to be invariant under the SRG transformation, the 3N short-range couplings c_D, c_E were fit in Ref. [7] for seven combinations of λ/Λ_{3N} to the experimental binding energy of ^{3}H and the charge radius of ^{4}He. The resulting values of the low-energy couplings are listed in Table I. This set of Hamiltonians serves as an estimate for the theoretical uncertainties due to nuclear forces in our many-body calculations.

The paper is organized as follows: In Sec. II, we introduce an improved density-dependent NN interaction to include 3N-force contributions in our calculations. In Sec. III, we discuss the expressions for the energy per particle to first and second order in many-body perturbation theory for general isospin asymmetries. In Sec. IV, we present our microscopic results for the energy per particle for eleven proton fractions based on a set of different Hamiltonians. We study their saturation properties, the incompressibility, symmetry energy, and also provide an analytic global fit of our results. Finally, we conclude and summarize in Sec. V.

II. IMPROVED NORMAL ORDERING

Normal ordering is a key step for the practical treatment of 3N forces as effective two-body interactions in many-body calculations of matter and nuclei. It allows us to rewrite the 3N-force part of the Hamiltonian exactly in terms of normal-ordered zero-, one- and two-body contributions plus a residual three-body term (for details see Ref. [3]). In infinite matter normal ordering involves a summation of one particle over occupied states in the Fermi sphere (see also Refs. [8,42]). For 3N forces this summation can be expressed formally in the form

$$\overline{V}_{3N} = \mathrm{Tr}_{\sigma_3}\mathrm{Tr}_{\tau_3}\int \frac{d\mathbf{k}_3}{(2\pi)^3} n^{\tau_3}_{\mathbf{k}_3} \mathcal{A}_{123} V_{3N}, \tag{2}$$

which involves sums over spin and isospin projection quantum numbers σ_3 and τ_3 as well as an integration over all momentum states, weighted by the momentum distribution functions $n^{\tau_3}_{\mathbf{k}}$ for a given neutron and proton density. In the following, we choose the Fermi–Dirac distribution function at zero temperature, $n^{\tau_3}_{\mathbf{k}} = \theta(k^{\tau_3}_F - |\mathbf{k}|)$, and we assume spin-unpolarized and homogeneous matter. We can apply the present framework also to general correlated distributions functions. However, it was shown in infinite matter [10] that the energy is not very sensitive to the particular choice of the reference state for the chiral EFT interactions used in this work. This indicates that the residual 3N contributions are very small such that they can be neglected. V_{3N} represents the 3N interaction, whereas $\mathcal{A}_{123}$ is the three-body antisymmetrizer. The effective interaction $\overline{V}_{3N}$ in Eq. (2) represents a density-dependent NN interaction that can be combined with contributions from free-space NN interactions.

The 3N interaction V_{3N} is the fundamental microscopic input to Eq. (2). The momentum dependence of a general translationally invariant 3N interaction can be most efficiently expressed as a function of the Jacobi momenta

$$\mathbf{p} = \frac{\mathbf{k}_1 - \mathbf{k}_2}{2}, \quad \mathbf{q} = \frac{2}{3}\left[\mathbf{k}_3 - \frac{1}{2}(\mathbf{k}_1 + \mathbf{k}_2)\right], \tag{3}$$

where $\mathbf{k}_i$ denote the single-nucleon momenta. In the following, $\mathbf{p}$ and $\mathbf{q}$ ($\mathbf{p}'$ and $\mathbf{q}'$) denote the Jacobi momenta of the initial (final) state:

$$V_{3N} = V_{3N}(\mathbf{p},\mathbf{q},\mathbf{p}',\mathbf{q}'). \tag{4}$$

Hence, it is natural to perform the normal ordering Eq. (2) in this Jacobi basis. By expressing all single-particle momenta in terms of the Jacobi momenta and the two-body center-of-mass momentum $\mathbf{P} = \mathbf{k}_1 + \mathbf{k}_2 = \mathbf{k}'_1 + \mathbf{k}'_2$ we obtain

$$\overline{V}_{3N} = \left(\frac{3}{2}\right)^3 \mathrm{Tr}_{\sigma_3}\mathrm{Tr}_{\tau_3}\int \frac{d\mathbf{q}}{(2\pi)^3} n^{\tau_3}_{(3\mathbf{q}+\mathbf{P})/2} \mathcal{A}_{123} V_{3N}. \tag{5}$$

The calculation of the effective interaction $\overline{V}_{3N}$ is challenging due to the complex structure of general 3N interactions. For practical treatment it is common to decompose 3N interactions in a Jj-coupled 3N partial-wave momentum basis of the form [43,44]

$$|pq\alpha\rangle \equiv |pq;[(LS)J(ls)j]\mathcal{J}(Tt)\mathcal{T}\rangle. \tag{6}$$

Here, L, S, J, and T denote the relative orbital angular momentum, spin, total angular momentum, and isospin of particles 1 and 2 with relative momentum p. The quantum numbers l, $s = 1/2$, j, and $t = 1/2$ label the orbital angular momentum, spin, total angular momentum, and isospin of particle 3 relative to the center-of-mass motion of particle 1 and 2. The 3N quantum numbers $\mathcal{J}$ and $\mathcal{T}$ define the total

3N angular momentum and isospin (for details see Ref. [43]). In particular, 3N interactions do not depend on the projection quantum numbers $m_{\mathcal{J}}$ and, for isospin-symmetric interactions, also not on $m_{\mathcal{T}}$, hence we omit these labels in the basis states.

We evaluate Eq. (5) in this partial-wave basis. The basic ingredient of our normal-ordering framework are antisymmetrized 3N matrix elements of the form

$$\langle pq\alpha|V_{3N}^{as}|p'q'\alpha'\rangle = \langle pq\alpha|(1+P_{123}+P_{132})V_{3N}^{(i)}(1+P_{123}+P_{132})|p'q'\alpha'\rangle, \quad (7)$$

where P_{123}, P_{132} are the cyclic permutation operators of three particles and $V_{3N}^{(i)}$ represents one Faddeev component of the 3N interaction (see Refs. [43,45] for details).

Previous normal-ordering frameworks for infinite matter have been developed for a specific 3N interaction, e.g., the leading chiral 3N interactions at N^{2}LO [8,42]. This makes it necessary to redevelop expressions for the effective interaction $\overline{V}_{3N}$ for each new contribution and for each isospin asymmetry. Moreover, the treatment of more complicated 3N interactions, e.g., the subleading chiral 3N interactions at N^{3}LO [34,35], becomes very tedious. In contrast, because the partial-wave decomposition of these 3N interactions has been completed very recently [45], these contributions can be included in the present framework without additional efforts.

Although the effective interaction $\overline{V}_{3N}$ is an effective NN interaction, there are important differences to free-space interactions: due to Galilean invariance, free-space NN interactions can only depend on the initial and final relative momenta $\mathbf{p}$ and $\mathbf{p}'$. Since the many-body rest frame defines a preferred frame the effective NN interaction $\overline{V}_{3N}$ generally also depends on the center-of-mass momentum $\mathbf{P}$. In particular, the interaction also depends on the angle between the momenta $\mathbf{p}$, $\mathbf{p}'$, and $\mathbf{P}$, which leads to a much more complicated partial-wave structure than for free-space NN interactions. In order to avoid these complications, the approximation $\mathbf{P}=0$ has been imposed for the effective NN interaction in previous works [8,10,42].

The flexibility of the present framework allows us to extend the calculation of $\overline{V}_{3N}$ to finite momenta $\mathbf{P}$. In order to reduce the complexity of the effective interaction and to simplify its application in many-body calculations we average the direction of $\mathbf{P}$ over all angles:

$$n^{\tau}_{(3\mathbf{q}+\mathbf{P})/2} \longrightarrow \Gamma^{\tau}(q,P) = \frac{1}{4\pi}\int d\Omega_{\mathbf{P}}\, n^{\tau}_{(3\mathbf{q}+\mathbf{P})/2}, \quad (8)$$

with

$$\Gamma^{\tau}(q,P) = \begin{cases} 1, & (3q+P) \leqslant 2k_{F,\tau} \\ 0, & |3q-P| \geqslant 2k_{F,\tau} \\ \frac{1}{2}\int_{-1}^{\gamma} d\cos\theta\, n^{\tau}_{(3\mathbf{q}+\mathbf{P})/2} & \text{otherwise,} \end{cases} \quad (9)$$

and $\gamma = (4k_{F,\tau}^2 - 9q^2 - P^2)/(6Pq)$. Within this approximation the effective interaction $\overline{V}_{3N}$ acquires an additional dependence on the absolute value of $\mathbf{P}$, whereas its partial-wave structure is still sufficiently simple so that it can be combined with free-space NN interactions in many-body calculations in a straightforward way. Explicitly, we obtain for the partial-wave matrix elements normalized to the direct term:

$$\begin{aligned}\langle p(LS)JTm_T|\overline{V}^{as}_{3N}(P)|p'(L'S')JT'm_T\rangle &= \frac{(-i)^{L'-L}}{(4\pi)^2}\left(\frac{3}{4\pi}\right)^3 3\int dqq^2 f_R(p,q)f_R(p',q) \\ &\times \sum_{\tau} \mathcal{C}^{\mathcal{T}m_T+\tau}_{Tm_T1/2\tau}\mathcal{C}^{\mathcal{T}m_T+\tau}_{T'm_T1/2\tau}\Gamma^{\tau}(q,P) \\ &\times \sum_{\substack{l,j \\ \mathcal{J},\mathcal{T}}} \frac{2\mathcal{J}+1}{2J+1}\delta_{ll'}\delta_{jj'}\delta_{JJ'}\,\langle pq\alpha|V^{as}_{3N}|p'q\alpha'\rangle\,, \end{aligned} \quad (10)$$

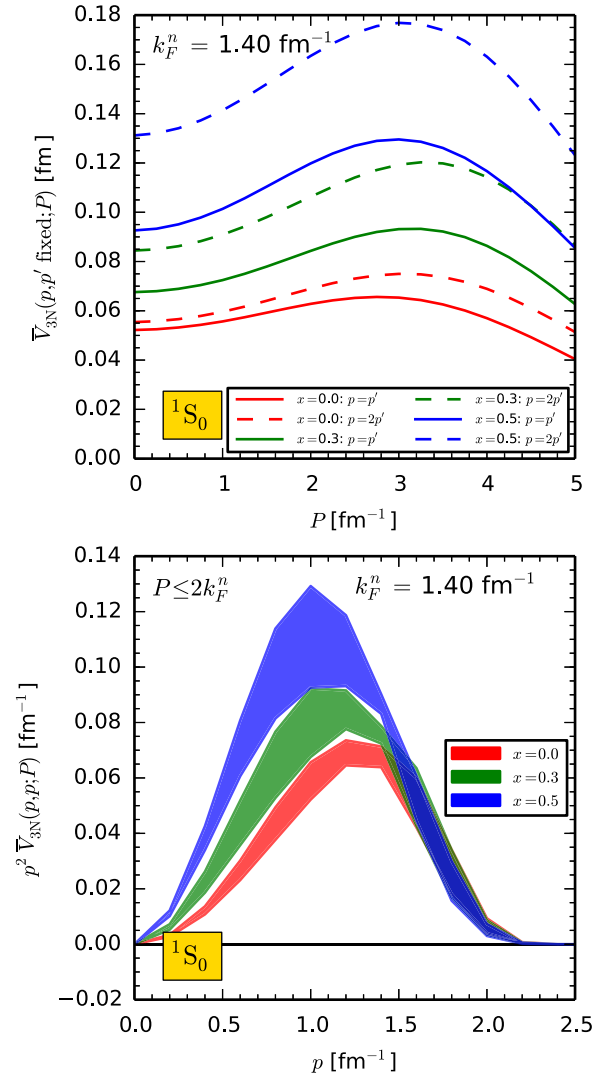

FIG. 1. The upper panel shows the matrix elements of the effective interaction $\overline{V}_{3N} = \overline{V}_{3N}/9$ in the $^1S_0$ channel with $m_T = -1$ as a function of the center-of-mass momentum P for fixed relative momenta, $p = p' = 1$ fm^{-1} (solid) and $p = 2p' = 1$ fm^{-1} (dashed line), and proton fractions x at a neutron Fermi momentum $k_F^n = 1.4$ fm^{-1}. For the color code, see the legend in the lower panel. The lower panel shows the diagonal matrix elements times p^2 as a function of the relative momentum p. In the first- and second-order many-body contributions, the value of P is kinematically limited to $P \leqslant k_F^{\tau_1} + k_F^{\tau_2}$, so for $m_T = -1$ to $P \leqslant 2k_F^n$.

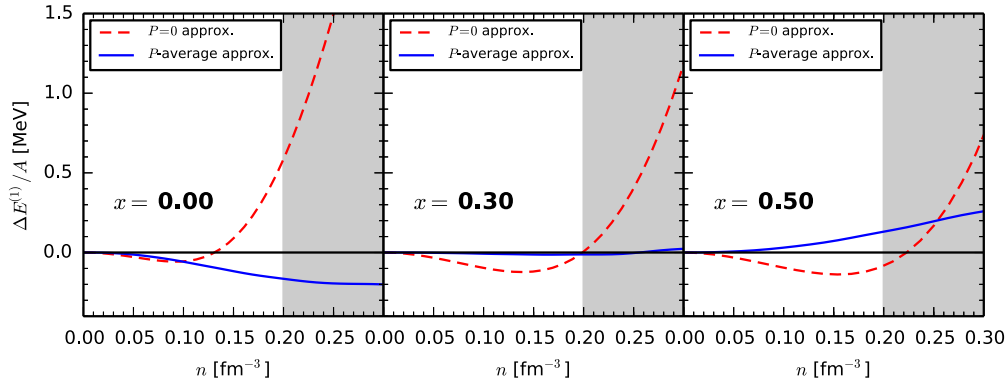

FIG. 2. Comparison of 3N Hartree–Fock energies based on Hamiltonian 2 in Table I for the $P = 0$ (red dashed) and P-average approximation (blue solid line) for the effective interaction $\overline{V}^{\rm as}_{\rm 3N}$. Results are shown as differences to the exact Hartree–Fock energy for three proton fractions, $x = 0$ (left), $x = 0.3$ (center), and $x = 0.5$ (right panel). The $P = 0$ values give larger deviations above saturation density, whereas the P-average approximation behaves more systematic over the entire density range.

where $f_{\rm R}(p,q)$ denotes the nonlocal 3N regulator function. We will use the form $f_{\rm R}(p,q) = \exp-\{[(p^2 + 3q^2/4)/\Lambda^2_{\rm 3N}]^4\}$ following Ref. [7]. Because of the definition of the 3N matrix elements in Eq. (7), our effective NN potential, $\overline{V}^{\rm as}_{\rm 3N} = \mathcal{A}_{123}\overline{V}_{\rm 3N}\mathcal{A}_{123}$, involves two antisymmetrizers, in contrast to the formal definition in Eq. (2).

Note that, except for neutron and symmetry matter, off-diagonal matrix elements in spin and isospin quantum numbers S and T contribute to the effective potential. It also depends on the isospin projection m_T, a direct consequence of the isospin dependence of the occupation function n^τ_k. Only in the case of neutron and symmetric nuclear matter is the interaction diagonal in S, T, and it is also independent of the allowed m_T because of isospin symmetry of chiral 3N forces up to N^{3}LO.

In Fig. 1 we present the results of some representative matrix elements of $\overline{V}_{\rm 3N} = \overline{V}^{\rm as}_{\rm 3N}/9$ in the ^{1}S$_0$ channel with $m_T = -1$ (nn) for different proton fractions x and a neutron Fermi momentum $k^n_F = 1.4$ fm^{-1}. The normalization of the matrix elements is chosen such that they can be directly combined with those of the free-space NN interaction for calculations in the Hartree–Fock approximation. The top panel shows the matrix elements at fixed relative momenta, $p = p' = 1$ fm^{-1} (solid) and $p = 2p' = 1$ fm^{-1} (dashed line), respectively, as a function of P. Due to momentum conservation, the value of P is kinematically limited to $P \leqslant k^{\tau_1}_F + k^{\tau_2}_F$ for the first- and second-order contributions, depending on $m_T = \tau_1 + \tau_2$. The lower panel shows the diagonal matrix elements with the measure p^2 as a function of the relative momentum for this range of center-of-mass momenta. The $P = 0$ results are in excellent agreement with Refs. [7,8]. For $x = 0$, the matrix elements have a rather weak dependence on P. This suggests that neutron matter results can be approximated reasonably well by the $P = 0$ approximation, as checked at the Hartree–Fock level in Ref. [8], while for increasing proton fractions the P dependence of the matrix elements becomes more pronounced.

In Fig. 2 we compare results for the 3N Hartree–Fock energies based on the different approximations for the effective NN interaction. The three panels show the energy difference to the exact Hartree–Fock result for proton fraction $x = 0$ (left), $x = 0.3$ (center), and $x = 0.5$ (right). The effective NN interaction based on the $P = 0$ approximation reproduces the exact results well up to $n \simeq (0.13$–$0.23)$ fm^{-3}, depending on the proton fraction. For higher densities, the deviation systematically increases, indicating a breakdown of the $P = 0$ approximation. In contrast, the results based on the P-average approximation agree well with the exact results over the entire density range.

III. MANY-BODY CALCULATIONS

For our many-body calculations we follow the calculation strategy of Ref. [26]. We parametrize the total density in terms

TABLE II. Coefficients $C_{\mu\nu}$ of the quadratic expansion (18) fit to the calculated equation of state $E/A(\beta,\bar{n})$ for each Hamiltonian. The values are from separately fitting neutron and symmetric nuclear and then extending quadratically in β according to Eq. (18). The coefficients are given in MeV.

	C_{02}	C_{03}	C_{04}	C_{05}	C_{06}	C_{22}	C_{23}	C_{24}	C_{25}	C_{26}
# 1	0.3	−66.1	79.2	−50.3	20.3	6.1	156.2	−306.0	259.3	−83.8
# 2	4.1	−78.2	92.5	−53.7	19.7	2.3	168.5	−319.9	263.8	−83.6
# 3	12.5	−125.2	191.0	−141.4	48.0	4.1	153.0	−275.9	209.2	−59.7
# 4	6.5	−83.0	92.8	−47.7	16.6	−0.2	174.5	−322.6	260.2	−81.2
# 5	9.1	−78.9	65.0	−13.2	4.2	−4.0	178.3	−311.7	240.0	−72.6
# 6*	2.2	−77.0	106.6	−76.7	28.8	−4.8	219.0	−440.3	377.1	−119.6
# 7	−0.9	−54.1	52.9	−28.5	17.6	−1.6	194.8	−385.0	332.9	−110.6

of the neutron Fermi momentum k_F^n and in terms of the proton fraction $x = n_p/n$ or, equivalently, the isospin asymmetry $\beta = (n_n - n_p)/n = 1 - 2x$. The neutron, proton, and total density are labeled as n_n, n_p, and $n = n_n + n_p$, respectively. We probe the sensitivity of our results to uncertainties of the Hamiltonian by performing calculations for all interactions listed in Table II. These Hamiltonians start from two different NN potentials, have different values of the SRG resolution scale λ, different 3N cutoffs Λ_{3N}, as well as different values of the long-range couplings c_i. In the future, the subleading 3N contributions as well as consistently evolved 3N forces up to N^{3}LO can be treated in the present framework once reliable fits for the couplings c_D, c_E are available. So far, fits based on present NN interactions lead to unnaturally large c_D, c_E couplings at N^{3}LO [46]. Work in this direction is currently in progress.

Our calculations are based on a perturbative expansion of the energy up to second order around the Hartree–Fock state. In the Hartree–Fock approximation, the energy density of isospin-asymmetric matter is given by

$$\frac{E_{\rm NN}^{(1)} + E_{\overline{3N}}^{(1)}}{V} = \frac{1}{4\pi^3}\int dpp^2 \int dP P^2 \sum_{m_T} f_{m_T}(\mathbf{p},\mathbf{P}) \sum_{L,S,J,T} (2J+1)[1-(-1)^{L+S+T}] \times \langle p(LS)JTm_T|V_{\rm NN} + \overline{V}_{3N}^{\rm as}(P)/9|p(LS)JTm_T\rangle, \tag{11}$$

with the short-hand notation $i = \mathbf{k}_i\sigma_i\tau_i$ and the combinatorial factor $(1/9)$ of the effective interaction $\overline{V}_{3N}^{\rm as}$ is discussed in detail in Ref. [8]. Note that, since the matrix elements in Eq. (7) involve two instead of one antisymmetrizer, a relative conversion factor of 3 is required for the comparison to Ref. [8]. Furthermore, we introduced the function $f_{m_T}(\mathbf{p},\mathbf{P}) = \int d\cos\theta_{\mathbf{p},\mathbf{p}} n^{\tau_1}_{\mathbf{P}/2+\mathbf{p}} n^{\tau_2}_{\mathbf{P}/2-\mathbf{p}}$, which depends only on the two-body isospin projection quantum number $m_T = \tau_1 + \tau_2$ because the integrand is symmetric in the isospin indices τ_1 and τ_2. It is important to constrain the phase-space integral to the nonvanishing region of the Fermi–Dirac distributions. The general case of the phase-space integral can be written as

$$I = \int_{-1}^{+1} d\cos\theta_{\mathbf{p},\mathbf{P}} n^{\tau_1}_{\mathbf{p}+\mathbf{P}/2} n^{\tau_2}_{\mathbf{p}-\mathbf{P}/2} f(\cos(\theta_{\mathbf{p},\mathbf{P}})) = \Theta(x_{\rm max} - x_{\rm min}) \int_{x_{\rm min}}^{x_{\rm max}} d\cos\theta_{\mathbf{p},\mathbf{P}} f(\cos(\theta_{\mathbf{p},\mathbf{P}})). \tag{12}$$

In terms of $D_i^{\pm}(p,P) \equiv (k_{F,\tau_i}^2 - P^2/4 - p^2)/(\pm pP)$, we obtain the limits,

$$x_{\rm min} = \max[-1.0, \min[+1.0, D_2^-(p,P)]], \tag{13a}$$

$$x_{\rm max} = \min[+1.0, \max[-1.0, D_1^+(p,P)]]. \tag{13b}$$

Since $f(\cos(\theta_{\mathbf{p},\mathbf{P}})) = 1$ at the Hartree–Fock level, this leads to $f_{m_T}(p,P) = (x_{\rm max} - x_{\rm min})\Theta(x_{\rm max} - x_{\rm min})$.

The second-order contribution to the energy density is given by

$$\frac{E_{\rm NN}^{(2)} + E_{\overline{3N}}^{(2)}}{V} = \frac{1}{4^2}\prod_{i=1}^{4}\left[{\rm Tr}_{\sigma_i}{\rm Tr}_{\tau_i}\int\frac{d\mathbf{k}_i}{(2\pi)^3}\right] \left|\langle 12|V_{\rm as}^{(2)}|34\rangle\right|^2 \frac{n^{\tau_1}_{\mathbf{k}_1} n^{\tau_2}_{\mathbf{k}_2}(1-n^{\tau_3}_{\mathbf{k}_3})(1-n^{\tau_4}_{\mathbf{k}_4})}{\varepsilon^{\tau_1}_{\mathbf{k}_1} + \varepsilon^{\tau_2}_{\mathbf{k}_2} - \varepsilon^{\tau_3}_{\mathbf{k}_3} - \varepsilon^{\tau_4}_{\mathbf{k}_4}} (2\pi)^3\delta(\mathbf{k}_1 + \mathbf{k}_2 - \mathbf{k}_3 - \mathbf{k}_4). \tag{14}$$

Expanding in partial waves and performing the spin sums leads to (see Refs. [8,47])

$$\begin{aligned}
&\sum_{S,S'M_S,M_{S'}} \langle \mathbf{p}SM_STM_T|V_{\rm as}^{(2)}|\mathbf{p}'S'M_{S'}T'M_T\rangle\langle \mathbf{p}'S'M_{S'}T''M_T|V_{\rm as}^{(2)}|\mathbf{p}SM_ST'''M_T\rangle \\
&= (4\pi)^2 \sum_{S,S'}(-1)^{S+S'}\sum_{\tilde L} P_{\tilde L}(\cos\theta_{\mathbf{p},\mathbf{p}'}) \sum_{L,L',\tilde L,\tilde L'}\sum_{J,\tilde J} i^{L-L'-\tilde L+\tilde L'}(-1)^{\tilde L+\tilde L'+L'} \mathcal{C}^{\tilde L 0}_{L'0\tilde L'0}\mathcal{C}^{\tilde L 0}_{L0\tilde L0} \begin{Bmatrix} L & S & J \\ \tilde J & \tilde L & \tilde L \end{Bmatrix}\begin{Bmatrix} \tilde L' & S' & \tilde J \\ J & \tilde L & \tilde L' \end{Bmatrix} \\
&\times (2J+1)(2\tilde J+1)\sqrt{(2L+1)(2L'+1)(2\tilde L+1)(2\tilde L'+1)}\langle k'(L'S')JT''M_T|V_{\rm as}^{(2)}|k(LS)JT'''M_T\rangle \\
&\times \langle k(\tilde L S)\tilde J T M_T|V_{\rm as}^{(2)}|k'(\tilde L'S')\tilde J T'M_T\rangle \\
&\times [1-(-1)^{\tilde L+S+T}][1-(-1)^{L'+S'+T''}][1-(-1)^{\tilde L'+S'+T'}][1-(-1)^{L+S+T'''}].
\end{aligned} \tag{15}$$

Here, the partial-wave interaction matrix elements are given by $V_{\rm as}^{(2)} = V_{\rm NN} + \overline{V}_{3N}^{\rm as}(P)/3$ (see Ref. [8]), resulting from the normal-ordered two-body part of 3N forces. $\{\ldots\}$ denote $6j$ symbols and $P_L(\cos\theta)$ are Legendre polynomials. The sums over the single-particle isospin quantum numbers have to be performed explicitly, because the Fermi–Dirac distribution functions break the isospin symmetry for asymmetric matter. We stress that, in general, the effective interaction $\overline{V}_{3N}$

couples different spin and isospin channels because of the isospin dependence of the Fermi–Dirac distribution functions in Eq. (5).

For the evaluation of Eq. (14) we need to calculate the single-particle energies $\varepsilon^{\tau}_{\mathbf{k}}$, which are in general determined by the solution of the Dyson equation $\varepsilon^{\tau}_{\mathbf{k}} = k^2/(2m) + \mathrm{Re}\Sigma^{\tau}(k,\varepsilon_{\mathbf{k}})$. For our calculations, we either use a free spectrum or compute the self-energy in the Hartree–Fock approximation and average over the external spin quantum numbers. Moreover, we average the isospin dependence, weighted by the proton fraction x,

$$\begin{aligned}\Sigma^{(1)}(k_1,x) = \frac{1}{2\pi}\int dk_2 k_2^2 \int d\cos\theta_{\mathbf{k}_1\mathbf{k}_2} \\ \times \sum_{T,M_T,\tau_1,\tau_2} w_{\tau_1}(x) n^{\tau_2}_{\mathbf{k}_2} \left(\mathcal{C}^{TM_T}_{1/2\tau_1 1/2\tau_2}\right)^2 \\ \times \sum_{J,S,L} (2J+1)[1-(-1)^{L+S+T}] \\ \times \langle k_{12}/2(LS)JTM_T|V_{\mathrm{NN}} \\ + \overline{V}^{\mathrm{as}}_{3\mathrm{N}}(P)/6|k_{12}/2(LS)JTM_T\rangle, \end{aligned} \tag{16}$$

with $k_{12} = |\mathbf{k}_1 - \mathbf{k}_2|$, and the combinatorial factor (1/6) of the effective interaction $\overline{V}^{\mathrm{as}}_{3\mathrm{N}}$ being discussed in Ref. [8]. The isospin weighting factor w_τ is given by

$$w_\tau(x) = \begin{cases} x, & \tau = +\frac{1}{2}\ \text{(proton)} \\ 1-x, & \tau = -\frac{1}{2}\ \text{(neutron)}. \end{cases} \tag{17}$$

In this approximation the single-particle energies for a certain proton fraction x are then $\varepsilon(k,x) = k^2/(2m) + \Sigma^{(1)}(k,x)$, with m being the average nucleon mass. In case of the free spectrum, we apply only the kinetic energy as single-particle energy. In neutron and symmetric matter, the isospin weighting is equivalent to the ones in Refs. [7,8] but includes also charge-symmetry breaking.

IV. RESULTS

A. Partial-wave convergence

For our practical calculations we include 3N matrix elements up to $\mathcal{J} = 9/2$ for the calculation of the effective interaction $\overline{V}_{3\mathrm{N}}$ via Eq. (10), where the 3N matrix elements are calculated in the framework of Ref. [45]. We checked that this basis space leads to well-converged results for the effective NN potential up to partial-wave channels with $J \lesssim 4$. In addition, we find excellent agreement with the matrix elements of $\overline{V}_{3\mathrm{N}}$ at $P = 0$ of Ref. [8] for neutron matter and with the corresponding results for symmetric nuclear matter [7] based on chiral 3N interactions at N^{2}LO.

As an additional benchmark we compare in Fig. 3 the Hartree–Fock contributions of 3N forces to the energy per particle based on a summation of 3N matrix elements using different truncations in $\mathcal{J}$ (following Ref. [48]) with results derived directly from evaluating the operatorial structure of the N^{2}LO 3N interactions (see Refs. [8,47]) for neutron matter (top panel) and for symmetric nuclear matter (lower panel). These two independent calculations test directly the convergence of the partial-wave decomposition and should provide identical results in the limit $\mathcal{J} \leqslant \mathcal{J}_{\max} \to \infty$ up to numerical uncertainties.

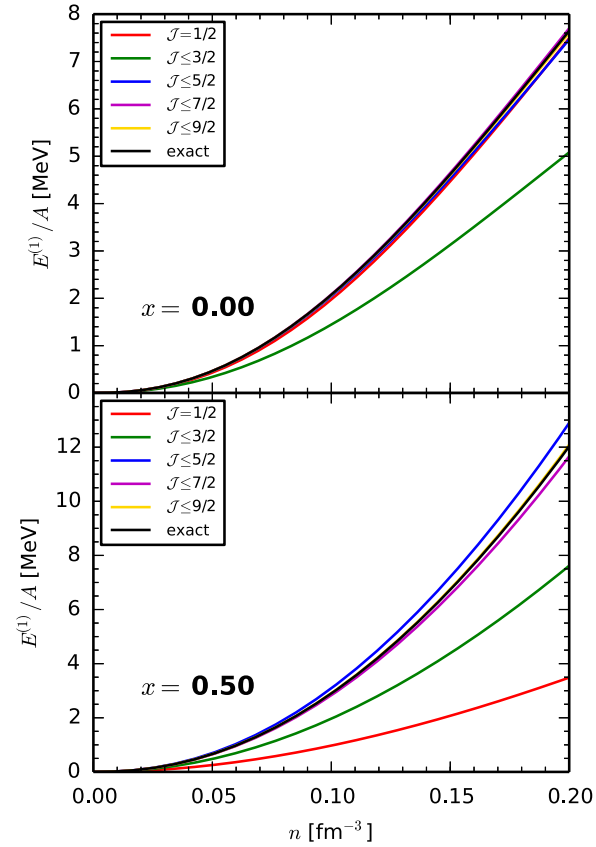

FIG. 3. Partial-wave convergence of the N^{2}LO 3N contributions at the Hartree–Fock level in neutron matter (top) and symmetric matter (bottom) for Hamiltonian 2 of Table I. For neutron matter the contributions for $\mathcal{J} > 5/2$ are very small, so the individual lines are nearly indistinguishable.

The results shown in Fig. 3 are based on the set of low-energy couplings of Hamiltonian 2 of Table I and by including all contributions with $J \leqslant 6$ for each 3N partial wave. We find excellent agreement of the results for $\mathcal{J} \leqslant 9/2$, with a deviation of less than 100 keV at saturation density for neutron matter and symmetric nuclear matter. Hence, for the following we will use this basis space for the calculation of the effective interaction $\overline{V}^{\mathrm{as}}_{3\mathrm{N}}$.

B. Discussion of equation of state

In Fig. 4, we show the results for the energy per particle for eleven proton fractions using different approximations for the single-particle energies and the effective interactions $\overline{V}_{3\mathrm{N}}$: the dashed lines show the results based on the free single-particle spectrum [i.e., $\Sigma^{(1)}(k_1,x) = 0$], whereas the solid lines show the results based on the single-particle energies calculated in the Hartree–Fock approximation; the colored (gray) bands represent results based on the effective NN potential calculated in the P-averaged ($P = 0$) approximation, respectively. For each of these four sets of results we determine

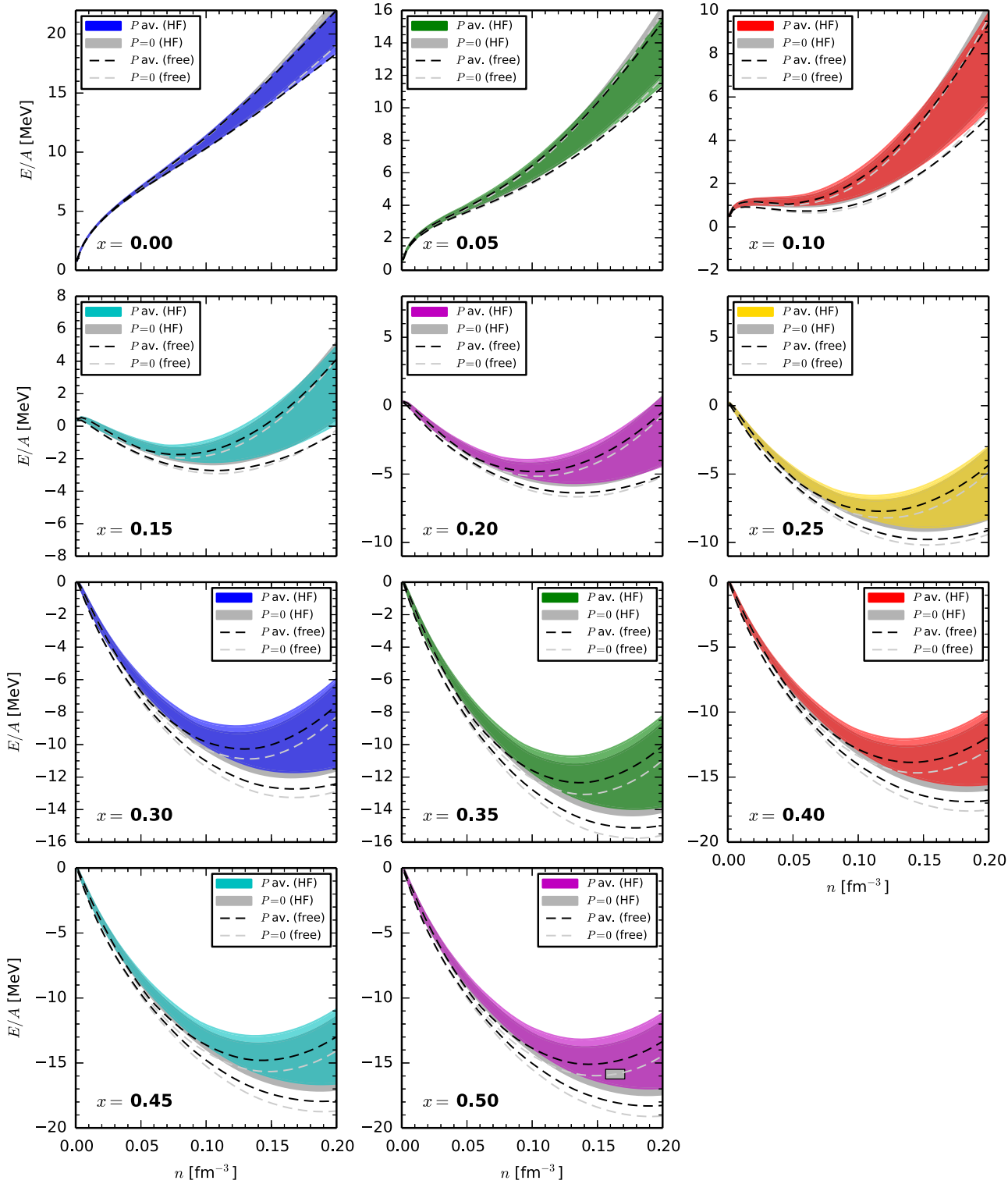

FIG. 4. Energy per particle of nuclear matter as a function of the total density $n = n_n + n_p$ for various proton fractions x. The two approximations of the effective NN potential, $P = 0$ and P average, and two approximations for the single-particle energies, free and Hartree–Fock, are shown. The energy range is based on the set of Hamiltonians listed in Table I. The excluded Hamiltonian 6* has no influence on the uncertainty bands. For a better view, the area between the dashed lines are not filled in the case of a free spectrum. For $x = 0.5$ we also show the empirical saturation point (see text for details).

the theoretical uncertainties by performing calculations based on the Hamiltonians listed in Table I and extract the maximal spread of these results. We note that, for Hamiltonian 6*, the fits of the short-range 3N couplings c_D,c_E in Ref. [7] have not taken into account the isospin breaking of the N^{3}LO NN potential EGM 550/600 MeV. This leads to deviations for the ^{3}H binding energy of ∼200 keV in comparison to exact calculations. We will discuss this Hamiltonian separately but emphasize here that it has no influence on the uncertainty bands shown in Fig. 4.

From the many-body point of view, neutron matter ($x = 0$) represents the simplest system. At N^{2}LO, only the long-range 3N forces proportional to c_1 and c_3 contribute for nonlocal regulators $f_R(p,q)$ due to the Pauli-principle and the isospin structure of the 3N forces [8]. In addition, no NN S-wave tensor interactions are active in neutron matter. As a result we find relatively narrow uncertainty bands with a width of about 4 MeV at saturation density.

Increasing the proton fraction influences the overall uncertainty in two ways: First, the width of the bands for each of the two single-particle spectra becomes larger up to 5 to 6 MeV for symmetric nuclear matter at the highest density shown. The upper uncertainty limit is always determined by Hamiltonian 7, which also leads to rather small saturation densities for $x = 0.5$ (see below). Second, the difference between the individual results based on the two spectra grows systematically for larger proton fractions. The dependence of our results on the single-particle energies probes the perturbativeness of the Hamiltonians and provides a measure of contributions from higher orders in the perturbative expansion. Hence, these results indicate the need to analyze third-order contributions more closely, which we discuss in Sec. IV C. The two approximations lead to comparable results and widely overlapping bands in each spectrum. We find that the P-average approximation is slightly more repulsive, and the bands are shifted at saturation density by ≈1 MeV in symmetric matter.

We discuss now the properties of the equation of state based on the P-average approximation of the effective interaction. Considering the free and the Hartree–Fock spectrum and, excluding Hamiltonian 6*, symmetric matter saturates at $n_0 = (0.138–0.190)$ fm^{-3} with energies of $E/A = -(13.2–18.3)$ MeV. Hamiltonian 6* increases slightly the upper limit by $\Delta n_0 = 0.003$ fm^{-3}. The saturation points for each of the seven Hamiltonians of Table I are shown in Fig. 5. The red (blue) points correspond to the calculations with a free (Hartree–Fock) spectrum. Hence, the gray line connecting the two calculations indicates the convergence of the calculation. We find a Coester-like linear correlation between the energy and density at the saturation point, but the range is considerably smaller than the Coester line based on NN interactions only [49]. The green band has been obtained by independently fitting a linear function to the saturation points for the two spectra excluding Hamiltonian 6*.

Skyrme energy-density functionals based on properties of nuclei and nuclear matter can be used to empirically constrain the saturation point [50–52]. Table 7 of Ref. [50] summarizes 16 selected functionals, which reproduce well selected properties of nuclear matter. Six more are excluded

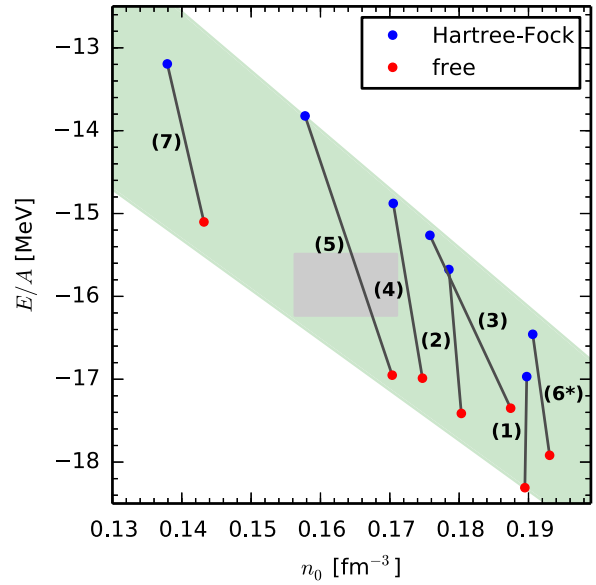

FIG. 5. Correlation between the saturation density and energy for the seven Hamiltonians of Table I, indicated by the figure. The green area highlights the obtained Coester band based on independently fitting the saturation points for a free and a Hartree–Fock spectrum. The gray lines connect the two spectra. As discussed in the text, the empirical saturation point (gray box) is given by the range of 14 selected energy-density functionals. The region is in good agreement with our calculated Coester band. See the text for details of Hamiltonian 6*.

because of unreasonable behavior for large densities [50] or being unstable for finite nuclei. The remaining ten are listed in Table 1 of Ref. [52]. Our empirical saturation range is determined based on these functionals plus those of Ref. [53] (SLy4, UNEDF0, UNEDF1, and UNEDF2). As a result we obtain the ranges $n_0^{\rm emp} = (0.164 \pm 0.007)$ fm^{-3} and $E^{\rm emp}/A \simeq -(15.9 \pm 0.4)$ MeV, which is indicated by the gray boxes in Figs. 4 (for $x = 0.5$) and 5.

Our band in Fig. 5, based on NN and 3N interactions, overlaps with the empirical saturation point, in contrast with calculations based on NN interactions only [49]. This holds especially for the equation of state based on Hamiltonian 4 and 5. We note that Hamiltonian 5 has the largest dependence on the spectrum as it is almost twice compared to Hamiltonian 1. This may be due to the large resolution scale $\lambda = 2.8$ fm^{-1} of the Hamiltonian. Although the ^{3}H binding energy corresponding to Hamiltonian 6* is not well fit, it behaves still natural and similar as Hamiltonian 1.

Following the usual quadratic expansion in the isospin asymmetry β, we approximate globally the equation of state in terms of a power series in the reduced density $\bar{n} = n/(0.16\ \text{fm}^{-3})$

$$\frac{E}{A}(\beta,\bar{n}) = \sum_{\substack{\mu=0,2 \\ \nu=2,3,4,5,6}} C_{\mu\nu}\beta^{\mu}\bar{n}^{\nu/3}. \qquad (18)$$

In order to determine the coefficients $C_{\mu\nu}$, we fit to the energy per particle of neutron and symmetric nuclear matter and

interpolate then quadratically in β to general isospin asymmetries. We constrain the fit to densities of (0.02–0.22) fm^{-3}. The resulting values of the coefficients are listed in Table II. Based on the root-mean-square deviation of the global energy expression and the equation of state of each calculated asymmetry, we have checked that Eq. (18) provides a reasonable approximation for our microscopic results, especially close to symmetric matter. At $n = 0.16$ fm^{-3}, the largest deviation to the data is $\lesssim$220 keV for neutron-rich matter, while the typical value for larger proton fractions is much smaller. We stress that these coefficients only represent results from a least-squares fit to our data and are given here just for completeness. In particular, any physical interpretation of these coefficients has to be done with care due to the large values of some coefficients (see Table II) and the resulting cancellations of terms.

Using the parametrization (18) we compute the incompressibility K and the symmetry energy S_v,

$$K = 9\frac{\partial^2}{\partial \bar{n}^2}\frac{E}{A}(\beta,\bar{n})\Big|_{\substack{\bar{n}=1,\\ \beta=0}} \tag{19a}$$

$$S_v = \frac{1}{2}\frac{\partial^2}{\partial \beta^2}\frac{E}{A}(\beta,\bar{n})\Big|_{\substack{\bar{n}=1,\\ \beta=0}} \tag{19b}$$

at the actual saturation density of each Hamiltonian. Based on the uncertainty ranges of our results (shown as the colored bands in Fig. 4) we obtain the ranges $K = (182–254)$ MeV and $S_v = (28.4–35.7)$ MeV, considering the free and the Hartree–Fock spectrum and excluding Hamiltonian 6*. Hamiltonian 6* would increase the upper uncertainty limits to $\Delta K = 8$ MeV and $\Delta S_v = 0.4$ MeV. We note that the value of $S_v = (30.2–32.2)$ MeV (at fixed density $n_0 = 0.16$ fm^{-3}), which we obtained in Ref. [26] for small proton fractions, is in agreement with these improved calculations. The uncertainty here is larger because Eqs. (19) are evaluated here at the actual saturation density of the Hamiltonian and not at fixed $n_0 = 0.16$ fm^{-3}. We will study the properties of the symmetry energy and the importance of a quartic term ($\sim\beta^4$) of the energy expansion in a subsequent presentation.

C. Estimate of third-order contribution

The results shown in Fig. 4 exhibit a mild sensitivity to the single-particle spectrum employed, which indicates that contributions beyond second order in the perturbative expansion might give non-negligible contributions. Here, we estimate third-order contributions to neutron and symmetric nuclear matter in order to assess the quality of the perturbative convergence. At third order, the diagrams involve particle-particle, hole-hole, and particle-hole excitations. We consider here only particle-particle and hole-hole diagrams, respectively (see Ref. [7] for details). The calculations are simplified by employing angle-averaged Fermi–Dirac distribution functions. Figure 6 shows the corresponding third-order contributions, $E^{(3)}/A$, in neutron (top panel) and symmetric matter (bottom panel) for the two approximations of the effective interaction and using free or Hartree-Fock single-particle energies.

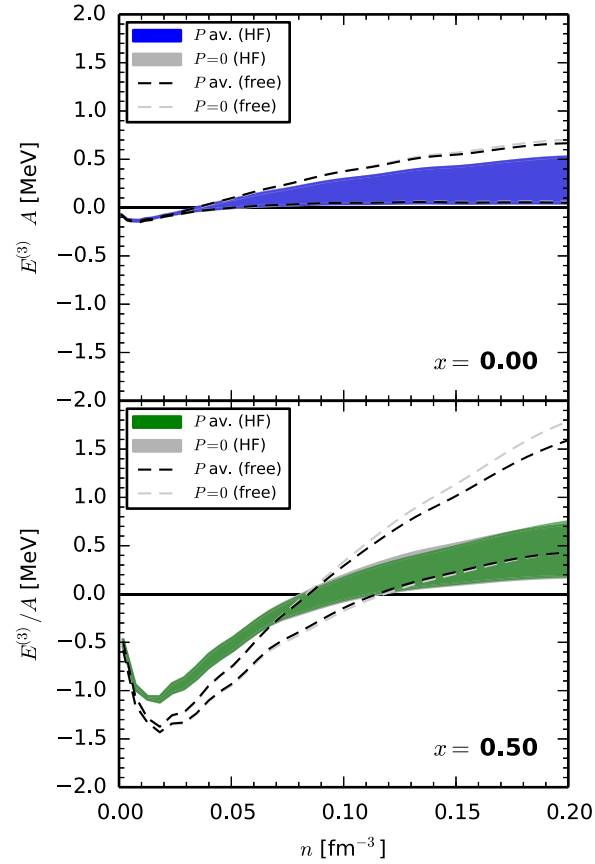

FIG. 6. Contributions at third order in the perturbative expansion to the energy of neutron matter (top panel) and symmetric nuclear matter (lower panel). The color coding and line styles are the same as in Fig. 4. Accordingly, the uncertainty estimates are based the Hamiltonians of Table I.

At $n_0 = 0.16$ fm^{-3} and using a Hartree–Fock (free) spectrum, we find repulsive contributions of up to ∼500 keV (∼600 keV) in neutron matter and ∼(100–600) keV [∼(0.3–1.3) MeV] in symmetric matter. The NN interaction dominates the overall contributions. However, 3N forces become more important for larger proton fractions. These findings are consistent with the results in Ref. [54], based on low-momentum interactions $V_{\mathrm{low}\,k}$. In future work, we will study the order-by-order convergence in the many-body expansion by including also particle-hole contributions (see also Ref. [14]). We emphasize that Hamiltonian 6* (see Table I) does not influence these uncertainty estimates.

In order to address the perturbative convergence we show in Fig. 7 for each Hamiltonian of Table I the energy contributions $\langle V\rangle/A$ to the free Fermi gas at first (red), second (green), and third order (blue) in many-body perturbation theory. The variation of the two single-particle spectra defines the uncertainty bands at second and third order. The figure shows that the second-order results are suppressed by a factor of ∼6 compared to Hartree Fock whereas the third-order estimates are suppressed by a factor of ∼5 relative to second order at the largest density shown, $n = 0.2$ fm^{-3}. The band at second order is typically ∼10% with respect to the first-order contribution.

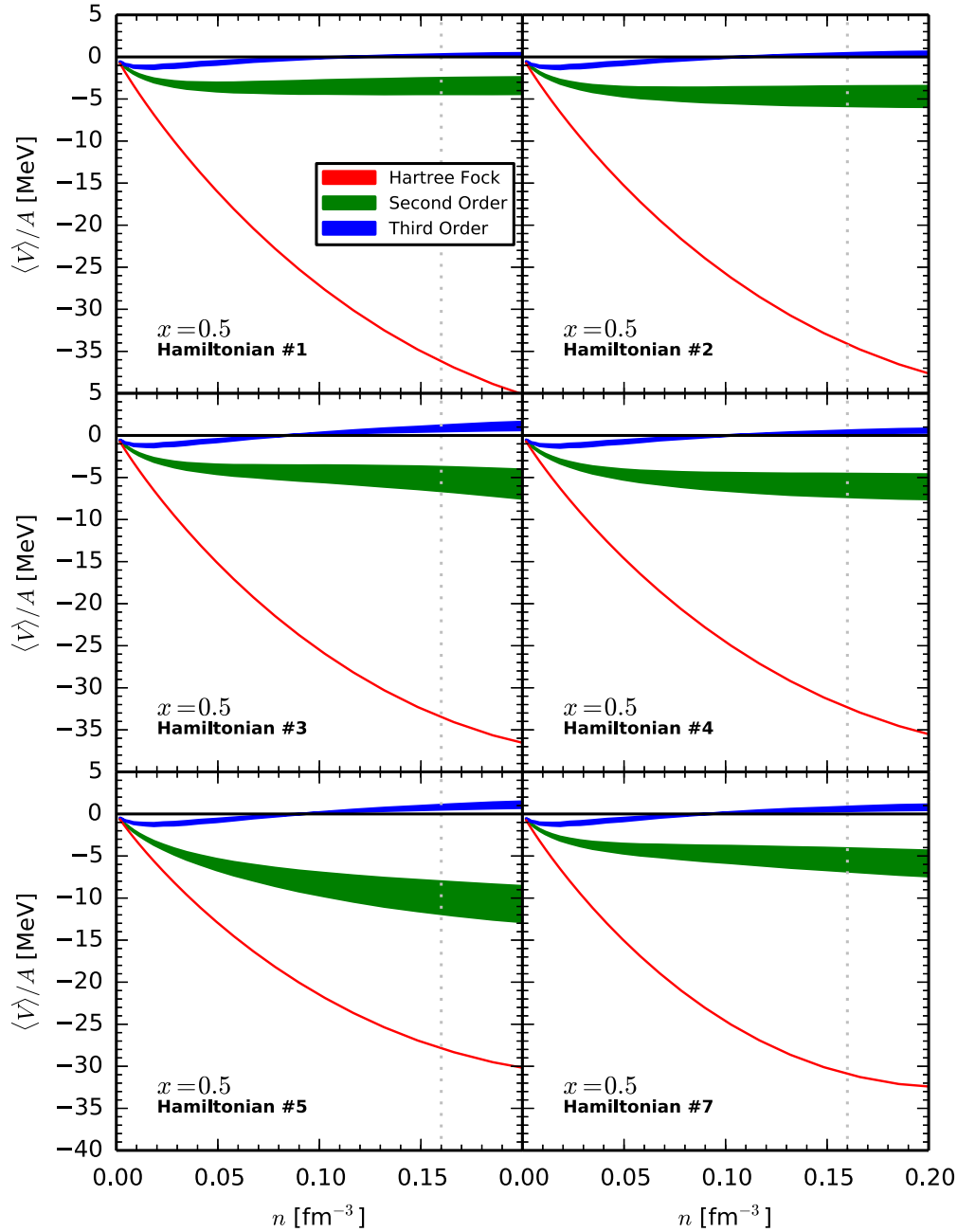

FIG. 7. Interaction energy at first, second, and third order in symmetric nuclear matter ($x = 0.5$) for the employed Hamiltonians of Table I. As discussed in the text Hamiltonian 6* is excluded. The suppression of higher orders in the perturbative expansion demonstrates the convergence of many-body perturbation theory and suggests that the sensitivity of the second-order results on the single-particle energies provide a conservative estimate for the many-body uncertainties.

Only the Hamiltonian (5) with the large resolution scale $\lambda = 2.8$ fm^{-1} shows, as expected, a larger sensitivity on the single-particle spectrum and a weaker suppression of higher-order terms in many-body perturbation theory.

In conclusion, Fig. 7 demonstrates the convergence of many-body perturbation theory for the employed Hamiltonians and suggests that the sensitivity of the second-order results on the single-particle energies provide a conservative estimate for the many-body uncertainties.

V. SUMMARY AND OUTLOOK

We presented results for isospin-asymmetric matter based on N^{3}LO NN and N^{2}LO 3N interactions calculated in many-body perturbation theory. The contributions from three-body forces beyond the Hartree–Fock approximation are included via an improved normal-ordering framework. This novel framework is based on partial-wave 3N matrix elements and makes it possible to generalize the computation of the effective

density-dependent two-body interaction to finite center-of-mass momenta. In addition, it is also straightforward to include contributions from subleading 3N interactions at N^{3}LO [34,35] by utilizing a new method for decomposing efficiently 3N interactions in a partial-wave plane-wave basis [45]. Such full N^{3}LO calculations can be performed immediately once reliable fits for the low-energy couplings c_D,c_E are available.

We employed the new normal-ordering framework to calculate the effective potential as a function of the center-of-mass momentum **P** by averaging this vector over all angles. We benchmarked our results against previous results for vanishing P and probed the sensitivity of the energy per particle at the Hartree–Fock level to different approximations in the normal ordering. We found that both approximations, $P = 0$ and P-averaging, provide good agreement with exact results up to intermediate densities of about $n \sim 0.13$ fm^{-3}, whereas the $P = 0$ approximation becomes unreliable beyond this density. In contrast, the new P-averaging approximation remains stable and close to the calculated results for all relevant densities.

For our many-body calculations we followed the strategy of Ref. [7]. The NN forces were evolved via the SRG, whereas the short-range couplings of the 3N interactions at N^{2}LO were fit to few-body observables at a given NN resolution scale. The theoretical uncertainties of our many-body observables are determined by the range obtained from the different Hamiltonians listed in Table I. Recently, this has been successfully used to study *ab initio* the charge radius, the neutron radius, the weak form factor, and the dipole polarizability of ^{48}Ca [55]. In addition, we estimated the many-body uncertainties by employing different approximations for the normal ordering of the 3N interactions and using different approximations for the single-particle energies.

Based on the results for the energies at different proton fractions, we fist calculated a global analytical fit in density and proton fraction for each Hamiltonian and then extracted results for the saturation point of symmetric matter, the incompressibility, and for the symmetry energy by using the standard quadratic expansion around symmetric matter. We found a Coester-like linear correlation between saturation density and energy, and the band covers the empirical range. In addition, we found that a quadratic parametrization in the isospin asymmetry reproduces the microscopic results reasonably well.

As next steps, it will be crucial to improve the estimates of the theoretical uncertainties and also to investigate different regulator choices. As an example, in Refs. [31,32] novel NN potentials at leading order (LO), next-to-leading order (NLO), N^{2}LO, N^{3}LO, and N^{4}LO and different regulator scales were derived. The present many-body framework allows to perform systematic order-by-order convergence studies in the chiral expansion at different regulator scales based on such potentials, including 3N forces up to N^{3}LO. In addition, the present framework can be generalized by performing the normal-ordering with respect to a general correlated reference state, by extending the calculations to finite temperature, and by incorporating particle-hole and higher-order contributions in the many-body expansion. This will allow also systematic convergence studies in the many-body expansion.

ACKNOWLEDGMENTS

We thank T. Krüger, J. M. Lattimer, and I. Tews for useful discussions. This work was supported by the ERC Grant No. 307986 STRONGINT and by the Deutsche Forschungsgemeinschaft through Grant SFB 1245.

[1] E. Epelbaum, H.-W. Hammer, and U.-G. Meißner, Rev. Mod. Phys. **81**, 1773 (2009).
[2] R. Machleidt and D. R. Entem, Phys. Rep. **503**, 1 (2011).
[3] S. K. Bogner, R. J. Furnstahl, and A. Schwenk, Prog. Part. Nucl. Phys. **65**, 94 (2010).
[4] R. J. Furnstahl and K. Hebeler, Rep. Prog. Phys. **76**, 126301 (2013).
[5] H.-W. Hammer, A. Nogga, and A. Schwenk, Rev. Mod. Phys. **85**, 197 (2013).
[6] K. Hebeler, J. D. Holt, J. Menendez, and A. Schwenk, Annu. Rev. Nucl. Part. Sci. **65**, 457 (2015).
[7] K. Hebeler, S. K. Bogner, R. J. Furnstahl, A. Nogga, and A. Schwenk, Phys. Rev. C **83**, 031301(R) (2011).
[8] K. Hebeler and A. Schwenk, Phys. Rev. C **82**, 014314 (2010).
[9] A. Carbone, A. Polls, and A. Rios, Phys. Rev. C **88**, 044302 (2013).
[10] A. Carbone, A. Rios, and A. Polls, Phys. Rev. C **90**, 054322 (2014).
[11] G. Hagen, T. Papenbrock, A. Ekström, K. Wendt, G. Baardsen, *et al.*, Phys. Rev. C **89**, 014319 (2014).
[12] A. Ekström, G. R. Jansen, K. A. Wendt, G. Hagen, T. Papenbrock, B. D. Carlsson, C. Forssén, M. Hjorth-Jensen, P. Navrátil, and W. Nazarewicz, Phys. Rev. C **91**, 051301 (2015).
[13] J. W. Holt, N. Kaiser, and W. Weise, Prog. Part. Nucl. Phys. **73**, 35 (2013).
[14] L. Coraggio, J. W. Holt, N. Itaco, R. Machleidt, L. E. Marcucci, and F. Sammarruca, Phys. Rev. C **89**, 044321 (2014).
[15] A. Gezerlis, I. Tews, E. Epelbaum, S. Gandolfi, K. Hebeler, A. Nogga, and A. Schwenk, Phys. Rev. Lett. **111**, 032501 (2013).
[16] A. Gezerlis, I. Tews, E. Epelbaum, M. Freunek, S. Gandolfi, K. Hebeler, A. Nogga, and A. Schwenk, Phys. Rev. C **90**, 054323 (2014).
[17] I. Tews, S. Gandolfi, A. Gezerlis, and A. Schwenk, Phys. Rev. C **93**, 024305 (2016).
[18] J. E. Lynn, I. Tews, J. Carlson, S. Gandolfi, A. Gezerlis, K. E. Schmidt, and A. Schwenk, Phys. Rev. Lett. **116**, 062501 (2016).
[19] K. A. Brueckner, S. A. Coon, and J. Dabrowski, Phys. Rev. **168**, 1184 (1968).
[20] I. E. Lagaris and V. R. Pandharipande, Nucl. Phys. A **369**, 470 (1981).
[21] I. Bombaci and U. Lombardo, Phys. Rev. C **44**, 1892 (1991).
[22] W. Zuo, I. Bombaci, and U. Lombardo, Phys. Rev. C **60**, 024605 (1999).
[23] W. Zuo, A. Lejeune, U. Lombardo, and J. Mathiot, Eur. Phys. J. A **14**, 469 (2002).

[24] I. Vidaña, C. Providência, A. Polls, and A. Rios, Phys. Rev. C **80**, 045806 (2009).
[25] T. Frick, H. Müther, A. Rios, A. Polls, and A. Ramos, Phys. Rev. C **71**, 014313 (2005).
[26] C. Drischler, V. Somà, and A. Schwenk, Phys. Rev. C **89**, 025806 (2014).
[27] C. Wellenhofer, J. W. Holt, and N. Kaiser, Phys. Rev. C **92**, 015801 (2015).
[28] N. Kaiser, Phys. Rev. C **91**, 065201 (2015).
[29] K. Hebeler, J. M. Lattimer, C. J. Pethick, and A. Schwenk, Astrophys. J. **773**, 11 (2013).
[30] R. J. Furnstahl, N. Klco, D. R. Phillips, and S. Wesolowski, Phys. Rev. C **92**, 024005 (2015).
[31] E. Epelbaum, H. Krebs, and U.-G. Meißner, Eur. Phys. J. A **51**, 53 (2015).
[32] E. Epelbaum, H. Krebs, and U.-G. Meißner, Phys. Rev. Lett. **115**, 122301 (2015).
[33] B. D. Carlsson, A. Ekström, C. Forssén, D. F. Strömberg, G. R. Jansen, O. Lilja, M. Lindby, B. A. Mattsson, and K. A. Wendt, Phys. Rev. X **6**, 011019 (2016).
[34] V. Bernard, E. Epelbaum, H. Krebs, and U.-G. Meißner, Phys. Rev. C **77**, 064004 (2008).
[35] V. Bernard, E. Epelbaum, H. Krebs, and U.-G. Meißner, Phys. Rev. C **84**, 054001 (2011).
[36] I. Tews, T. Krüger, K. Hebeler, and A. Schwenk, Phys. Rev. Lett. **110**, 032504 (2013).
[37] T. Krüger, I. Tews, K. Hebeler, and A. Schwenk, Phys. Rev. C **88**, 025802 (2013).
[38] K. Hebeler, Phys. Rev. C **85**, 021002(R) (2012).
[39] D. R. Entem and R. Machleidt, Phys. Rev. C **68**, 041001(R) (2003).
[40] E. Epelbaum, W. Glöckle, and U.-G. Meißner, Nucl. Phys. A **747**, 362 (2005).
[41] M. C. M. Rentmeester, R. G. E. Timmermans, and J. J. de Swart, Phys. Rev. C **67**, 044001 (2003).
[42] J. W. Holt, N. Kaiser, and W. Weise, Phys. Rev. C **81**, 024002 (2010).
[43] W. Glöckle, *The Quantum Mechanical Few-Body Problem* (Springer, Berlin, Heidelberg, 1983).
[44] R. Skibiński, J. Golak, K. Topolnicki, H. Witała, H. Kamada, W. Glöckle, and A. Nogga, Eur. Phys. J. A **47**, 48 (2011).
[45] K. Hebeler, H. Krebs, E. Epelbaum, J. Golak, and R. Skibiński, Phys. Rev. C **91**, 044001 (2015).
[46] J. Golak, R. Skibiński, K. Topolnicki, H. Witała, E. Epelbaum, H. Krebs, H. Kamada, U.-G. Meißner, V. Bernard, P. Maris, J. Vary, S. Binder, A. Calci, K. Hebeler, J. Langhammer, R. Roth, A. Nogga, S. Liebig, and D. Minossi, Eur. Phys. J. A **50**, 177 (2014).
[47] L. Tolos, B. Friman, and A. Schwenk, Nucl. Phys. A **806**, 105 (2008).
[48] K. Hebeler and R. J. Furnstahl, Phys. Rev. C **87**, 031302 (2013).
[49] F. Coester, S. Cohen, B. Day, and C. M. Vincent, Phys. Rev. C **1**, 769 (1970).
[50] M. Dutra, O. Lourenço, J. S. Sá Martins, A. Delfino, J. R. Stone, and P. D. Stevenson, Phys. Rev. C **85**, 035201 (2012).
[51] B. A. Brown, Phys. Rev. Lett. **111**, 232502 (2013).
[52] B. A. Brown and A. Schwenk, Phys. Rev. C **89**, 011307 (2014).
[53] M. Kortelainen, J. McDonnell, W. Nazarewicz, E. Olsen, P.-G. Reinhard, J. Sarich, N. Schunck, S. M. Wild, D. Davesne, J. Erler, and A. Pastore, Phys. Rev. C **89**, 054314 (2014).
[54] S. K. Bogner, A. Schwenk, R. J. Furnstahl, and A. Nogga, Nucl. Phys. A **763**, 59 (2005).
[55] G. Hagen, A. Ekström, C. Forssén, G. R. Jansen, W. Nazarewicz, T. Papenbrock, K. A. Wendt, S. Bacca, N. Barnea, B. Carlsson, C. Drischler, K. Hebeler, M. Hjorth-Jensen, M. Miorelli, G. Orlandini, A. Schwenk, and J. Simonis, Nat. Phys. **12**, 186 (2016).